Inorganic Chemistry

pubs.acs.org/IC Article

Biotin−Pt(IV)−Ru(II)−Boron−Dipyrromethene Prodrug as "Platin Bullet" for Targeted Chemo- and Photodynamic Therapy

Arpan Bera, Amrita Nepalia, Aarti Upadhyay, Deepak Kumar Saini,* and Akhil R. Chakravarty*

Cite This: *Inorg. Chem.* 2024, 63, 17249−17262 Read Online

ACCESS | Metrics & More | Article Recommendations | Supporting Information

ABSTRACT: Using the principle of "Magic Bullet", a cisplatin-derived platinum(IV) prodrug heterobimetallic **Pt(IV)−Ru(II)** complex, *cis,cis,trans*-$[Pt(NH_3)_2Cl_2\{Ru(tpy{-}BODIPY)(tpy{-}COO)\}(biotin)]Cl_2$ (**Pt−Ru−B**, **2**), having two axial ligands, namely, biotin as water-soluble B-vitamin for enhanced cellular uptake and a BODIPY−ruthenium(II) (**Ru−B**, **1**) photosensitizer having *N,N,N*-donor tpy (4′-phenyl-2,2′:6′,2″-terpyridine) bonded to boron-dipyrromethene (BODIPY), is developed as a "Platin Bullet" for targeted photodynamic therapy (PDT). **Pt−Ru−B** exhibited intense absorption near 500 nm and emission near 513 nm (λ_{ex} = 488 nm) in a 10% dimethyl sulfoxide-Dulbecco's phosphate-buffered saline medium (pH 7.2). The BODIPY complex on light activation generates singlet oxygen as the reactive oxygen species (ROS) giving a quantum yield (Φ_Δ) of ∼0.64 from 1,3-diphenylisobenzofuran experiments. **Pt−Ru−B** exhibited preferential cellular uptake in cancer cells over noncancerous cells. The dichlorodihydrofluorescein diacetate assay confirmed the generation of cellular ROS. Confocal images revealed its mitochondrial internalization. **Pt−Ru−B** showed submicromolar photocytotoxicity in visible light (400−700 nm) in A549 and multidrug-resistant MDA-MB-231 cancer cells. It remained nontoxic in the dark and less toxic in nontumorigenic cells. Cellular apoptosis and alteration of the mitochondrial membrane potential were evidenced from the respective Annexin V-FITC/propidium iodide assay and JC-1 dye assay. A wound healing assay using A549 cells and **Pt−Ru−B** revealed inhibition of cancer cell migration, highlighting its potential as an antimetastatic agent.

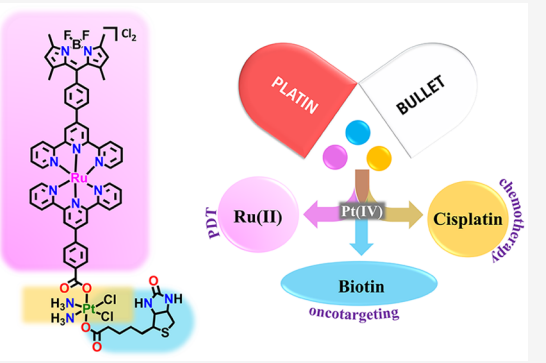

INTRODUCTION

Cisplatin and related platin analogues are clinically approved anticancer drugs.[1−4] Their therapeutic efficacy is largely affected by the inherent or acquired drug resistance due to the absence of desirable selectivity.[5−7] To circumvent these predicaments, six-coordinate kinetically stable $5d^6$-Pt(IV) prodrugs derived from cisplatin are developed as alternatives.[8−10] The pseudo-octahedral Pt(IV) complexes with their remarkable stability ensure better circulation within the bloodstream, thus minimizing the undesired reactivity that is often encountered by planar cisplatin with labile Pt−Cl bonds. Moreover, two axial ligands in these Pt(IV) prodrugs offer a versatile platform for customization, facilitating the incorporation of additional functionalities by allowing attachment of a tumor targeting group for better selectivity, and a photosensitizer (PS) for type-II PDT (photodynamic therapy) activity (Figure 1).[11−14] Targeted drug delivery being an important concept of "Magic Bullet", coined by Paul Ehrlich in 1907 for better efficacy and to reduce unwanted toxicity, is applicable for the Pt(IV) prodrug design where a cancer cell targeting group could be tagged in one axial position, while a photosensitizer is appended at the other axial site for better therapeutic efficacy.[15] We have recently shown that a Pt(IV) prodrug bearing boron-dipyrromethene (BODIPY) as a photosensitizer and vitamin biotin as two axial ligands significantly enhances the photocytotoxicity of the prodrug.[16] A related work showed that binding of Ru(II) to biotin and BODIPY in a heteroleptic complex significantly increases the generation of singlet oxygen compared to the Pt(IV)-based prodrug.[17] This has prompted us to conceptualize a new heterobimetallic prodrug molecule, namely, {Biotin−Pt(IV)−Ru(II)−tpy−BODIPY} where Pt(IV) is bonded to biotin and the {Ru(II)−tpy−BODIPY} moiety (**1**) as a photosensitizer through a tpy−COO^- linker. Thus, a heterobimetallic *cis,cis,trans*-$[Pt(NH_3)_2Cl_2\{Ru(tpy{-}BODIPY)(tpy{-}COO)\}(biotin)]Cl_2$ (**Pt−Ru−B**, **2**) complex is designed and prepared with an aim to release concomitantly two axial ligands from the Pt(IV) prodrug on reduction forming: (i) {Ru(tpy−BODIPY)(tpy−COO)} (**1**, **Ru−B**) for PDT activity, (ii) biotin as therapeutically active molecule, and (iii) the chemoactive cisplatin analogue (Figure 1). The {**Biotin−Pt(IV)···Ru(II)−tpy−BODIPY**} single molecular system in complex **2**

Received: July 22, 2024
Revised: August 22, 2024
Accepted: August 26, 2024
Published: September 5, 2024

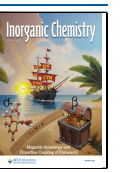

https://doi.org/10.1021/acs.inorgchem.4c03083
Inorg. Chem. 2024, 63, 17249−17262

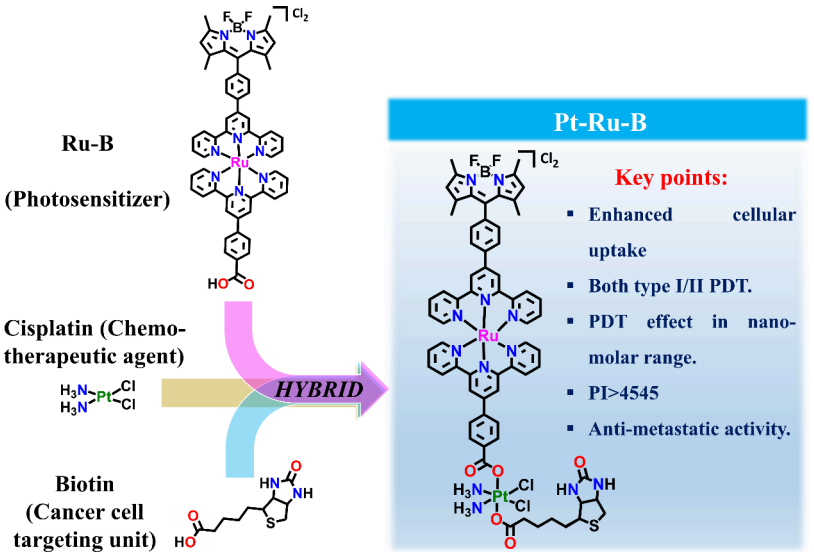

Figure 1. Chemical structure of the complex *cis,cis,trans*-$[Pt(NH_3)_2Cl_2\{Ru(tpy{-}BODIPY)(tpy{-}COO)\}(biotin)]Cl_2$ (**Pt−Ru−B**) and the concept behind the design of this prodrug. **Pt−Ru−B** generated chemo-active cisplatin and the photosensitizer upon reduction. The significant observations of this study are given as an inset (key points).

has two potentially labile axial linkers that can be cleaved readily by reducing agents with a two-electron Pt(IV) → Pt(II) reduction. This molecular design has proven to be significantly more effective than the {**Biotin−Ru(II)−tpy−BODIPY**} in **1** where a cleavage of the constituent bonds cannot be effected by an external trigger.

The choice of a photosensitizer (PS) in PDT is very important. Cisplatin cores that are covalently linked to porphyrin/phthalocyanine dyes are used to achieve triple action light-activated cytotoxicity, namely, chemotherapy, PDT, and cancer immunotherapy.[18,19] Guo and co-workers reported the conjugation of a red-light active PDT agent with a cisplatin analogue as a chemotherapeutic agent in photo-chemotherapy.[20] "Photoactivated Chemotherapy" (PACT) as a new methodology is based on a Pt(IV) prodrug that on light activation releases two axial ligands generating cytotoxic species in a controlled manner increasing drug efficacy.[21] The PACT methodology offers further scope of molecular design by incorporating PDT-active axial ligand, while a tumor targeting moiety could be at the other axial site thus allowing one to have a dual "Chemo-PDT" effect from a single molecular platform on light activation. The effectiveness of PDT using organic porphyrin dyes is limited by sluggish diffusion rates, short lifetimes of the ROS, and the lack of targeted delivery at the diseased cells besides skin sensitivity and hepatotoxicity.[22−28] We have chosen a BODIPY (boron-dipyrromethene) dye as a photosensitizer for its remarkable photo- and redox stability. Moreover, BODIPY cores are amenable to modifications allowing one to have optimal absorption and emission properties required for cellular imaging with high fluorescence quantum yield (Φ_F) and/or submicromolar PDT activity with high singlet oxygen quantum yield (Φ_Δ).[29−31] Inclusion of two heavy metals, namely, Ru(II) and Pt(IV), within a single molecular framework is intended for cumulative or potentially cooperative outcomes with high Φ_Δ values as recently reported for Pt(IV)−Ru(II) polypyridyl prodrugs by Gasser et al. while simultaneously exhibiting anticancer and imaging properties with organelle-targeting capabilities, as evidenced in an Ir(III)−Pt(IV) prodrug reported by Sasmal et al.[32,33] Zhu et al. reported non-photoactive Pt(IV)−Ru(II)−arene complexes, while Gibson et al. documented Pt(IV)−Au(I) complexes in their studies.[34a,b] Our choice of biotin in **2** is to enhance the solubility and cell targeting properties of the complex as biotin-tagged Pt(IV) complexes reported by Guo and co-workers showed targeted activity in breast cancer cells.[35] Herein, we present the chemo-PDT activity of a biotinylated heterobimetallic Pt(IV)−Ru(II) prodrug (**2**) derived from cisplatin and the **Ru−B** complex **1** (Scheme 1). Significant results include: (i) photocytotoxicity at submicromolar complex concentration involving singlet oxygen as the ROS, (ii) high prodrug uptake in cancer cells compared to the normal cells, (iii) preferential mitochondrial localization, (iv) high molar extinction coefficient of the visible band and high Φ_Δ value, and (v) observation of antimetastatic activity. Complex **2** presents a rare single molecular platform that rapidly generates three therapeutically active constituents on reduction.

RESULTS AND DISCUSSION

Synthesis and General Properties. The precursor complex, *cis,cis,trans*-$[Pt(NH_3)_2Cl_2(OH)_2]$ (Oxoplatin), was prepared using a technique previously described by Dhar et al.[36] Following previously published protocols, ligand tpy−BOD ($\mathbf{L^1}$) was synthesized involving a reaction of 2,4-dimethyl pyrrole and tpy−CHO (tpy, terpyridine) in dichloromethane, while tpy−COOH ($\mathbf{L^2}$) was synthesized from 2-acetylpyridine and 4-formyl benzoic acid reaction (Schemes S1 and S2, Supporting Information).[17,37] As shown in Scheme 1, ligand $\mathbf{L^1}$ was first reacted with $[Ru(DMSO)_4Cl_2]$ in an alcoholic solution, which resulted in the formation of $[Ru\mathbf{L^1}(DMSO)Cl_2]$ as an intermediate (Scheme S3, Supporting Information). This ruthenium intermediate was then treated with $\mathbf{L^2}$ to produce the ruthenium−bis-terpyridine complex in moderate yield. The synthetic procedure for the pseudo-octahedral $5d^6$-Pt(IV) metallodrug {**Pt−Ru−B**} is presented in Scheme 1.

Our attempt for direct substitution of two axially bound hydroxyl groups in Oxoplatin by the carboxyl group of biotin and the $^-$OOC−tpy−**Ru−B** complex gave undesirable reactivity. Therefore, activation of the carboxyl group for

https://doi.org/10.1021/acs.inorgchem.4c03083
Inorg. Chem. 2024, 63, 17249−17262

Scheme 1. Synthetic Scheme for the Complexes Ru−B (1) and Pt−Ru−B (2): (i) EtOH, 80°C, N_2 Atmosphere and (ii) TBTU, TEA, Dry DMF, 45°C, 48 h[a]

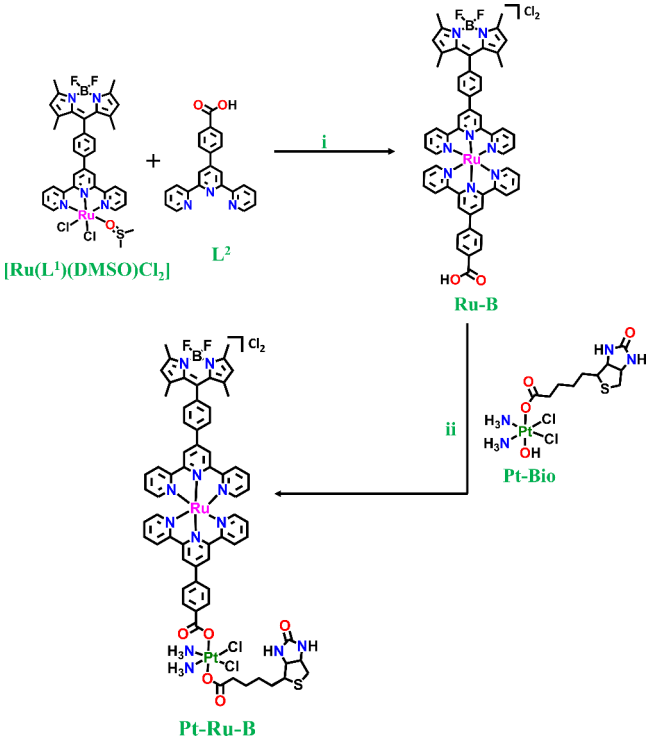

[a]Reagents used: EtOH, 2-(1*H*-benzotriazole-1-yl)-1,1,3,3-tetramethylaminium tetrafluoroborate (TBTU), triethylamine (TEA), and *N*,*N*-dimethylformamide (DMF).

both biotin and the **Ru−B** unit was achieved using either 1-(3-(dimethylamino)propyl)-3-ethylcarbodiimide hydrochloride and *N*-hydroxy succinimide or 2-(1*H*-benzotriazole-1-yl)-1,1,3,3-tetramethylaminium tetrafluoroborate (TBTU). Multinuclear NMR techniques ^{1}H, ^{13}C, and ^{11}B and ESI-MS were used to characterize the prodrug **Pt−Ru−B** and **Ru−B** complex. Selected physicochemical data are presented in Table 1 (Figures S1−S14, Supporting Information). The purity of the complexes was ascertained from the elemental analysis data. DMSO-d_6 was used for NMR spectroscopy of the complexes. On purification by column chromatography, the complexes were isolated in the form of their chloride salts. The singlet ^{1}H NMR spectral peaks observed between δ ∼2.5 and 1.5 were assigned to the pyrrole −CH_3 protons, along with a peak near δ 6.29, which was assigned to the pyrrole −CH proton. The Pt(IV)-bonded NH_3 protons appeared as a broad signal within 6.81−6.68 ppm.[35] The aliphatic −CH_2− protons that are specific to the biotin moiety appeared as a broad signal extending from 1.67 to 1.31 ppm. The resonance signals of the aromatic carbon were observed in the range of 116−163 ppm. At 0.67 ppm, a peak with characteristic features was observed in the ^{11}B NMR spectrum. The electrospray ionization mass spectrometry (ESI-MS) in methanol of the complexes gave a prominent peak assignable to the $[M\text{-}2Cl]^{2+}$ species. The isotopic distribution analysis revealed a variation of 0.5 in the m/z value suggesting dipositive nature of the species.[38] Furthermore, comparing the experimental isotopic distribution to the simulated counterpart has led to the identification of the species. The complexes are 1:2 electrolytic giving molar conductance values of ∼140 S m^2 mol^{-1} in dimethylformamide (DMF) indicating their dipositive nature.[39]

Photophysical Properties. The UV−visible absorption spectra of prodrug **Pt−Ru−B** and complex **Ru−B** in a solvent mixture of 10% DMSO and DPBS exhibited a strong absorption band centered around 500 nm with high molar extinction coefficient values (Figure 2a). The distinctive

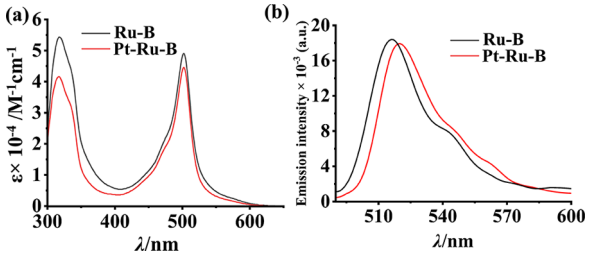

Figure 2. (a) UV−visible absorption and (b) emission spectra (λ_{ex} = 488 nm) of complex **Ru−B** and **Pt−Ru−B** in a 10% DMSO/DPBS medium (pH = 7.2) (color code: black, complex **Ru−B** and red, **Pt−Ru−B**).

electronic absorption arises from a spin-allowed $\pi-\pi^*$ transition within the BODIPY framework, which imparts a sharp characteristic to the spectrum.[40] Additionally, the prominent peak includes a Ru(II)-dπ to terpyridine (tpy)-π^* (MLCT) transition. This latter appears as a minor hump on the higher-energy region of the UV−visible spectra. The absorption observed within 300−400 nm is a result of the $\pi-\pi^*$ transitions occurring within the polypyridyl subunits.[41] Using 488 nm excitation, the emission spectra of the complexes were recorded in a mixture of 10% DMSO/DPBS

Table 1. Selected Physicochemical Data for Complexes Ru−B and Pt−Ru−B

entry	Ru−B (1)	Pt−Ru−B (2)
UV−visible: λ_{max}/nm (ε/M^{-1} cm^{-1})[a]	317 (5.42 × 10^4), 478 (2.18 × 10^4), 500 (4.88 × 10^4)	316 (4.15 × 10^4), 477 (2.02 × 10^4), 500 (4.43 × 10^4)
emission: λ_{em}/nm[b] (Φ_F)	512 (<0.01)	513 (<0.01)
Φ_Δ ($^1O_2$)[c]	0.63	0.64
^{1}H NMR chemical shift (δ, ppm) of γ-proton of BODIPY[d]	6.29	6.29
Λ_M[e]/S m^2 mol^{-1}	138	141
CV data[f]: Pt(IV)−Pt(II) (E_{pc}/V), BODIPY {E_f/V) [ΔE_p/mV]}, Ru(III)/Ru(II) (E_{pa}/V)	−1.64 V (65 mV), −2.06 V (82 mV), +0.78 V	−1.41 V, −1.72 V (75 mV), −2.19 V (132 mV), +0.72 V

[a]In a 10% DMSO/DPBS medium. sh, shoulder. [b]Emission wavelength and fluorescence quantum yield (Φ_F). The excitation wavelength (λ_{ex}) = 630 nm. [c]Singlet oxygen quantum yield Φ_Δ in DMSO. The value for tpy−BODIPY is 0.06. [d]In DMSO-d_6. [e]Molar conductivity in DMF. [f]E_f (V vs Fc/Fc^+), ΔE_p values at a scan rate of 100 mV s^{-1}. E_{pa} and E_{pc} are the anodic and cathodic peak potential, respectively, at a scan rate of 100 mV s^{-1}. E_f is 0.5 × (E_{pa} + E_{pc}).

https://doi.org/10.1021/acs.inorgchem.4c03083
Inorg. Chem. 2024, 63, 17249−17262

(Figure 2b). Notably, the complexes exhibited a subdued emission centered at around 513 nm, with a fluorescence quantum yield (Φ_F) value below 0.01. The quenching in BODIPY fluorescence observed in these complexes is attributed to the facile intersystem crossing (ISC) due to the presence of heavy metal atoms platinum and ruthenium.

Electrochemistry. The Pt(IV)-based prodrugs are known to exhibit a characteristic one-step two-electron transfer process leading to the conversion of pseudo-octahedral d^6-Pt(IV) to planar d^8-Pt(II) species.[42] To investigate the redox behavior of the present complexes, cyclic voltammetry (CV) experiments were performed in an anhydrous DMF solvent using tetrabutylammonium hexafluorophosphate (TBAHP) as the supporting electrolyte (Table 1). The **Ru−B** complex gave a distinct and irreversible Ru(II) to Ru(III) oxidation process near +0.78 V vs Fc/Fc^+ similar to those reported for $[Ru(tpy)_2]^{2+}$.[43] The **Ru−B** complex in the cathodic scan exhibited a BODIPY-based quasi-reversible voltammetric response at −1.64 V (ΔE_p = 65 mV at 100 mV s^{-1}) (Figures S15 and S16, Supporting Information). Another cathodic response observed at −2.06 V is attributed to the reduction of the terpyridyl ligand bound to the Ru(II) center. The **Pt−Ru−B** complex showed similar redox properties as in **Ru−B** with the exception that it exhibited an additional voltammetric response characterized by an irreversible cathodic process assignable to a one-step, two-electron transfer Pt(IV) to Pt(II) reduction (Figure S15, Supporting Information). This redox response occurred at a potential of −1.41 V (vs Fc/Fc^+) at a scan rate of 100 mV s^{-1}. The irreversibility of this process is due to a structural change resulting from the dissociation of two axial ligands from the six-coordinate $5d^6$-Pt(IV) prodrug, leading to the formation of a four-coordinate $5d^8$-Pt(II) species. The absence of an anodic peak corresponding to the observed cathodic peak at various scan rates suggested the involvement of an electron transfer with a simultaneous chemical transformation (EC) mechanism in this metal-mediated redox process.[44] While this Pt-based redox process occurred beyond the biological potential window of +0.4 to −0.4 V (vs SCE), the redox transformation could still be achieved through chemical reduction of the complex.

Theoretical Studies. Density Functional Theory (DFT) calculations were conducted using Gaussian 09W to elucidate both the structural characteristics and photophysical properties of the **Pt−Ru−B** complex.[45,46] The Pt(IV) core is surrounded by six ligands adopting a *cis,cis,trans* pseudo-octahedral arrangement, having two axial Pt−O bonds with a length of 2.04 Å (Figures S17 and S18 and Tables S1 and S2, Supporting Information). The boron atom within the BODIPY unit adopts a tetrahedral geometry. HOMO−LUMO diagrams were constructed based on optimized geometry. Notably, the HOMO is situated on the biotin moiety, while the LUMO is centered on the ruthenium component. The energy difference between the HOMO and LUMO states is 1.03 eV. Employing time-dependent density functional theory (TD-DFT), theoretical calculations were performed to predict the electronic transitions within the **Pt−Ru−B** complex. Key findings obtained from these calculations are presented in Table S3 in the Supporting Information. The **Pt−Ru−B** complex gave a λ_{max} value of 486 nm with a good oscillator strength of 0.28 in DMSO, and this data is consistent with the experimentally observed λ_{max} value of 500 nm.

Solubility and Stability. The complexes exhibit good solubility in various solvents, including dimethylformamide, dimethyl sulfoxide, methanol, and ethanol. The complexes are moderately soluble in acetonitrile and essentially insoluble in hydrocarbons and diethyl ether. The complexes show low solubility in water and an aqueous buffer. The stability of the prodrug **Pt−Ru−B** under physiological conditions was studied by absorption spectroscopy. The complexes in the dark showed good stability in a mixture of 10% dimethyl sulfoxide (DMSO) and DPBS buffer (pH, 7.2) over a period of 48 h with negligible reduction of the absorption intensity at 500 nm (Figure S19, Supporting Information). The photostability of the prodrug was investigated with the same solvent mixture, using a broadband photoreactor of 400−700 nm as the light source, and the complexes showed only a marginal reduction in absorption intensity, suggesting their good photostability (Figure S20, Supporting Information). Furthermore, stability studies were conducted under different pH conditions, specifically at high pH of 9 and low pH of 4. In both cases, prodrug **Pt−Ru−B** exhibited negligible changes in absorbance throughout the 48 h duration. The observed stability under highly acidic conditions implies the potential for oral administration in clinical treatments (Figure S21, Supporting Information).

Prodrug Activation. The prodrug is designed to release three distinct therapeutically important species with specific functionalities upon intracellular Pt(IV) → Pt(II) reduction.[47] First species is cisplatin or its analogue, a chemotherapeutic agent known for its anticancer properties. The second species is a ruthenium−BODIPY dyad, which exhibits remarkable PDT activity, enabling the generation of reactive oxygen species upon light activation. The third species is biotin, which is tagged to facilitate cancer cell targeting and enhance the selectivity of the prodrug toward the cancer cells. Together, they work synergistically to provide a multidimensional modality for cancer treatment. The release of the components was studied by ESI-MS spectrometry. To investigate the redox transformation of the prodrug, a DMSO-d_6 solution containing the prodrug at a concentration of 100 μM was subjected to a 24 h incubation period in the presence of sodium ascorbate (500 μM), which is a cellular reducing agent. Following the incubation, the resulting solution was analyzed by using ESI-MS in diluted HPLC methanol. The ESI-MS data showed the presence of reduction products such as unbound Ru−bis-terpyridine complex with BODIPY, biotin, and cisplatin species (Figure S22, Supporting Information). The prodrug was incubated at a concentration of 100 μM with 500 μM sodium ascorbate, and subsequently, the mixture was exposed to visible light (400−700 nm, 10 Joules/cm^2). Similarly, peaks were observed for the unbound ruthenium−bis-terpyridine complex alongside its conjugates with BODIPY, biotin, and cisplatin (Figure S23, Supporting Information). However, when subjected solely to light exposure (400−700 nm, 10 Joules/cm^2), the mass peak corresponding to the **Pt−Ru−B** complex remained unchanged even after 24 h of continuous illumination (Figure S24, Supporting Information). The prodrug seemed to be reduced only in the presence of chemical reductants. Additionally, to replicate the intracellular DNA binding characteristic of the released cisplatin, a truncated model of DNA known as 9-ethylguanine (9-EtG) was added to a small portion of the sodium ascorbate-incubated sample. The analysis of mass spectra in HPLC methanol indicated the presence of a Pt(II)-9-EtG adduct, specifically $[Pt(NH_3)_2Cl(9\text{-EtG})]^+$ (m/z = 444.0695), suggest-

https://doi.org/10.1021/acs.inorgchem.4c03083
Inorg. Chem. 2024, 63, 17249−17262

ing the formation of a complex of cisplatin with 9-EtG (Figure S25, Supporting Information).

Light-Induced Singlet Oxygen Generation. To assess the potential of the complexes in generating singlet oxygen ($^1O_2$) upon light activation, a trap experiment was conducted using 1,3-diphenylisobenzofuran (DPBF), which serves as a scavenger that readily reacts with singlet oxygen to form endoperoxide.[48] This reaction leads to a reduction in the intensity of the DPBF-based absorption band, typically observed at around 417 nm. The singlet oxygen quantum yield (Φ_Δ) for both **Pt−Ru−B** and **Ru−B** was determined by analyzing the graph of ΔOD (change in optical density) plotted against light irradiation time. Rose Bengal (RB) was used as a standard (Φ_Δ ~0.76 in DMSO). Using this approach, the Φ_Δ values for **Pt−Ru−B** and **Ru−B** were 0.64 and 0.63, respectively (Figure 3a, Figure S26, Supporting Information).

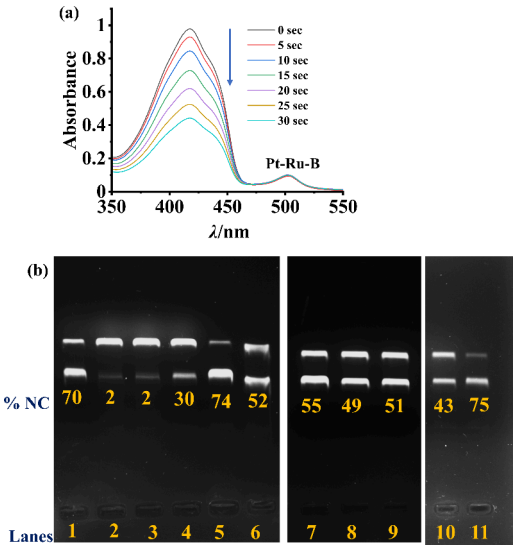

Figure 3. (a) Reduction in the absorption spectral intensity of DPBF at 417 nm in the presence of **Pt−Ru−B** (**2**) (light source: 400−700 nm photoreactor). The spectra were recorded at 5 s time intervals. (b) Gel electrophoresis image showing photocleavage of pUC19 DNA by complex **2** (10 μM) upon 532 nm green diode laser exposure for 5 min. Lanes are (1) DNA + **2** in light, (2) DNA control in light, (3) DNA + **2** in dark, (4) DNA + **2** + NaN_3 (6 μM) in light, (5) DNA + **2** + KI (6 μM) in light, (6) DNA + **2** + Tiron (6 μM) in light, (7) DNA + **2** + SOD (4 units) in light, (8) DNA + **2** + TEMP (6 μM) in light, (9) DNA + **2** + DHN (6 μM) in light, (10) DNA + **2** in argon under light irradiation, and (11) DNA + **2** + catalase (4 units) in light.

The values are remarkable considering the Φ_Δ value of ligand tpy−BODIPY as only 0.06, which is significantly low compared to the complexes highlighting the heavy metal effect in singlet oxygen generation and the utility of heavy metal for enhanced PDT activity.[49]

DNA Photocleavage and the Nature of ROS. Photodynamic therapy (PDT) relies on the generation of reactive oxygen species (ROS). There exist two primary mechanistic pathways, known as type-I PDT and type-II PDT, each contributing differently to the therapeutic effect. The type-I process is based on an electron transfer mechanism with biomolecules. This process leads to the formation of peroxides, hydroxyl radicals, and superoxide anion radicals. In a type-II process, the excited triplet state of the photosensitizer can directly transfer energy to molecular triplet oxygen ($^3O_2$), resulting in the production of highly toxic singlet oxygen ($^1O_2$).[50] The advantage of singlet oxygen in PDT is that there are no naturally occurring enzymes specifically designed to neutralize or counteract this ROS. As a result, singlet oxygen produced through this pathway can exert its potent effects within a confined range, making it an advantageous strategy for targeted therapeutic applications. To ascertain the type of ROS generated, supercoiled (SC) plasmid DNA served as a probe in the experiments. The experimental setup involved utilizing a 10 μM concentration of the **Pt−Ru−B** complex and a 400−700 nm visible light photoreactor as the light source for irradiation. Upon light exposure of the prodrug in the presence of SC pUC19 DNA, a significant conversion of the DNA from its supercoiled form to ~70% nicked circular (NC) form was observed (Figure 3b). The presence of hydroxyl radicals (such as potassium iodide) and peroxide radical scavengers (catalase) resulted in only minor changes in the DNA scission activity of the prodrug. However, singlet oxygen quenchers such as sodium azide (NaN_3), 2,2,6,6-tetramethyl-4-piperidone (TEMP), and 1,5-dihydroxynaphthalene (DHN) resulted in a significant decrease in the percentage of NC formation. The DNA photocleavage data suggest the formation of singlet oxygen during the DNA photocleavage process. The addition of Tiron and SOD (superoxide radical scavenger) also showed some inhibitory effects, indicating their involvement in a type-I pathway. The literature reports have shown that photoexcited Ru(II)-organic chromophore dyads display similar electron transfer reactions with biological substrates.[51] Overall, the results indicate production of both superoxide and singlet oxygen by the prodrug from the respective type-I and type-II photosensitization processes.

In previous reports, the utility and importance of molecular oxygen in PDT were observed from an experiment under argon that showed a significant decrease in the %NC DNA formation. Despite this reduced %NC, photoinduced DNA cleavage was still evident from the experiment suggesting the possibility of cleavage under hypoxic conditions without involving any ROS but from direct interaction with the biomolecule.[52,53]

Cellular Uptake. The cellular uptake of the prodrug in A549 cancer cells was investigated from a flow cytometry experiment at various time intervals of 2, 4, 5, and 6 h. The fluorescence was measured by using an excitation wavelength of 495 nm. The molecule's capability to penetrate and accumulate within the cancer cells is vital for its anticancer activity. A notable increase in the fluorescence intensity of the cells treated with the complex provided clear evidence of the internalization and accumulation of the metallodrug within the cancer cells. Furthermore, a significant enhancement in the fluorescence intensity was observed with an extended incubation time, specifically from 2 to 4 h, suggesting an increased uptake and retention of the prodrug over time. Notably, the complex exhibited time-dependent enhancement in cellular uptake, and the peak of incorporation was achieved following a 4 h incubation period (Figure 4a). To investigate the cancer cell targeting efficacy of the compound **Pt−Ru−B**, the cellular uptake was examined in both cancerous A549 cells and noncancerous Beas-2B cells. More positive shift in the histogram, determined from the histogram median value, was observed in A549 cells, which signifies a stronger uptake of the drug for cancer cells in comparison to normal cells (Figure 4a for A549 cells and Figure 4b for Beas-2B cells). In addition, various experiments were conducted to gain insights into the

https://doi.org/10.1021/acs.inorgchem.4c03083
Inorg. Chem. 2024, 63, 17249−17262

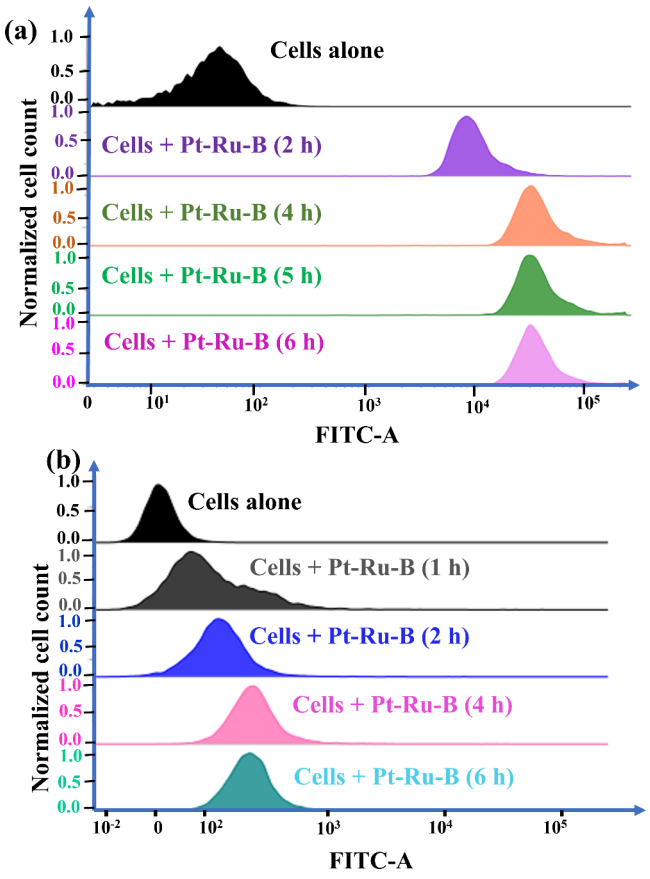

Figure 4. Cellular uptake analysis by flow cytometry for A549 (a) and Beas-2B (b) cells that were incubated with **Pt−Ru−B** (10 μM) at 37 °C for 4 h. The higher shift in the band position for **Pt−Ru−B** in cancerous A549 cells in panel a compared to Beas-2B cells in panel b indicates higher cellular uptake in the cancer cells than in the normal cells. Untreated cells were used as a control.

cellular uptake pathway of the prodrug. The cellular uptake of **Pt−Ru−B** was found to be significantly reduced when the cells were preincubated with biotin, suggesting the involvement of multivitamin transporters (SMVTs) in facilitating the cellular incorporation of the prodrug (Figure S27, Supporting Information). To emphasize the cancer cell targeting capability of the prodrug, the cellular uptake was examined in both cancerous A549 cells and noncancerous Beas-2B cells derived from the same tissue of origin, specifically the lungs.

Photocytotoxicity. The evaluation of cytotoxicity of **Pt−Ru−B** and **Ru−B** was carried out using the MTT (3-(4,5-dimethylthiazol-2-yl)-2,5-diphenyltetrazolium bromide) assay. The cytotoxicity of the complexes induced by light was assessed on three cell lines: A549 (human lung adenocarcinoma), MDA-MB-231 (human epithelial breast adenocarcinoma), and Beas-2B (human nontumorigenic lung epithelial cell line).[16] The selection of the A549 cell line was based on its overexpression of sodium-dependent multivitamin transporter (SMVT) receptors, while the MDA-MB-231 cell line was chosen for its inherent multidrug resistance property.[54,55] Additionally, to confirm the targeted photodynamic effect of the prodrug on cancer cells compared to normal cells, the cytotoxicity of the prodrug was also assessed in Beas-2B normal cells.

The experimental procedure involved incubation of the cells with increasing concentrations of the complexes for a duration of 4 h, after which they were subjected to light treatment. Simultaneously, a separate set of experiments were conducted without light treatment to determine the inherent cytotoxicity of the molecules. Subsequently, the cells were incubated for an additional 20 h, followed by the determination of the half-maximum inhibitory concentration (IC_{50}) using the MTT assay. During the light treatment, the photosensitizers were activated by a visible light source (400−700 nm photoreactor) using a light dose of approximately 5 Joules/cm^2 for a duration of 15 min. In the tested cell lines, the complexes were nontoxic nature in the absence of photoactivation as evidenced from the IC_{50} values exceeding 100 μM. Upon photoactivation, the biotin-conjugated prodrug yielded an IC_{50} value of ∼0.022 μM in A549 and ∼0.050 μM in MDA-MB-231 cancer cells (Figure 5, Table 2). In contrast, under similar conditions, **Ru−B**

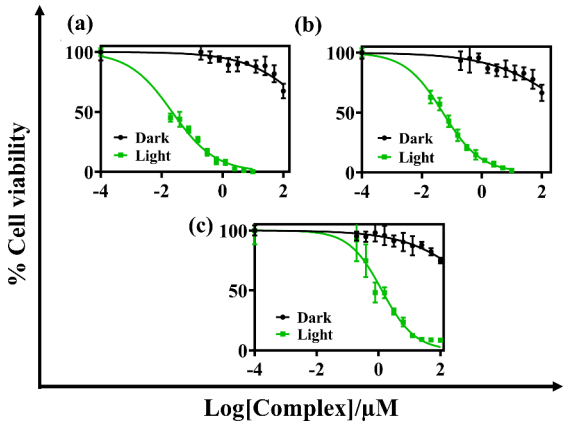

Figure 5. Cell viability profiles from the MTT assay of **Pt−Ru−B** in (a) A549 cells, (b) MDA-MB-231 cells, and (c) Beas-2B cells on light exposure (green light photoreactor of 400−700 nm, dosage: 5 Joules/cm^2) and in darkness (black).

Table 2. Photocytotoxicity (in μM) of Pt−Ru−B Prodrug (2) and Ru−B Complex (1)[a]

entry	A549/light[a] [dark] (PI)	MDA-MB-231/ light[a] [dark] (PI)	Beas-2B/light[a] [dark] (PI)
Pt−Ru−B	0.022 ± 0.004 [>100] (>4545)	0.050 ± 0.003 [>100] (>2000)	1.29 ± 0.20 [>100] (>77)
Ru−B	0.295 ± 0.060 [>100] (>338)	0.545 ± 0.050 [>100] (>183)	1.88 ± 0.50 [>100] (>53)
cisplatin + Ru−B + biotin[b]	0.280 ± 0.083 [34.24 ± 1.6] (122)	0.537 ± 0.06 [92.32 ± 1.3] (172)	1.99 ± 0.04 [55.68 ± 2.5] (28)
cisplatin[c]	32.5 ± 2.5 [35.0 ± 2.2]		

[a]Light source for **Pt−Ru−B** and **Ru−B** was a Luzchem photoreactor (λ = 400−700 nm, dose: 5 Joules/cm^2). PI is photocytotoxicity index [PI = IC_{50} (dark)/IC_{50} (light)]. A549 and MDA-MB-231 are the cancer cells, while Beas-2B was used as a normal cell. [b]A mixture of cisplatin, complex **Ru−B**, and biotin in a 1:1:1 molar ratio. [c]Data taken from ref 16.

exhibited relatively higher IC_{50} values ranging from 0.30 to 0.55 μM (Figure S28, Supporting Information). No cytotoxicity was observed in the Beas-2B cell line under dark conditions, indicating its inactivity. The photocytotoxicity index (PI), which is determined by calculating the ratio of dark and light IC_{50} values, serves as a measure of the therapeutic efficacy of a drug in PDT. A higher PI value signifies a reduced occurrence of off-site toxicity caused by the administered

https://doi.org/10.1021/acs.inorgchem.4c03083
Inorg. Chem. 2024, 63, 17249−17262

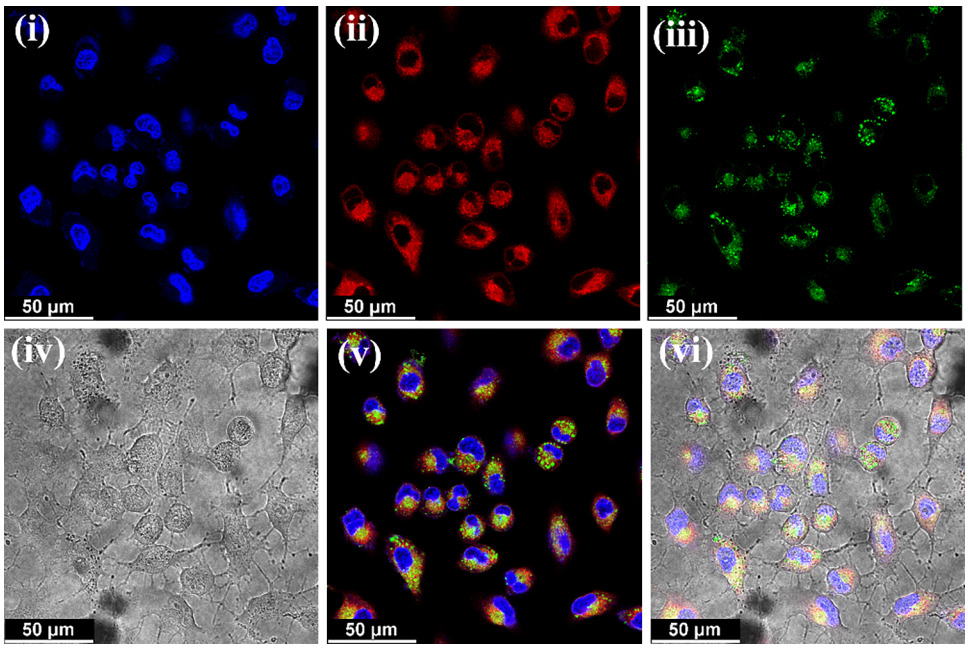

Figure 6. Confocal microscopy images of complex **Pt−Ru−B** in A549 cells recorded after 4 h of incubation using nuclear staining Hoechst dye and Mito Tracker Red: (i) Hoechst dye, (ii) Mito Tracker Red, (iii) complex **Pt−Ru−B**, (iv) bright field, (v) merged without bright field, and (vi) merged image with a bright field. The scale bar is 50 μm. Panel v indicates significant mitochondrial localization of the prodrug.

photosensitizer. In the cancerous A549 cell line, **Pt−Ru−B** exhibited a remarkable PI value exceeding 4500. However, in the nontumorigenic Beas-2B cells, the PI value was significantly low at ∼77, implying a reduced phototoxicity. Furthermore, an MTT assay was done on the A549, MDA-MB-231, and Beas-2B cells using a combination of cisplatin, biotin, and **Ru−B** in a 1:1:1 molar ratio (Figure S28, Supporting Information). The IC_{50} values observed under light conditions were 0.28, 0.54, and 1.98 μM, respectively, whereas under dark conditions, the respective IC_{50} values were 34.24, 92.32, and 55.68 μM. Our previously reported compound gave IC_{50} values between 0.61 and 1.54 μM in the tested cancer cell lines when exposed to light at wavelengths of 600−720 nm with a light dose of 30 Joules/cm^2 and exhibited a photocytotoxicity index within 65−163. This significant enhancement in cytotoxicity is attributed to the increased singlet oxygen production due to the altered coordination environment of the BODIPY photosensitizer, specifically the polypyridyl system of ruthenium rather than its direct coordination to the Pt−OH bond. A related study involving a heteroleptic biotin-containing BODIPY−Ru−bis-terpyridine complex gave an IC_{50} value of 0.16 μM in A549 cancer cells under visible light exposure with a dose of 2.2 Joules/cm^2 and a lower PI value ∼625 when compared to over 4545 obtained in this work. The MTT assay results strongly suggest the synergistic action of **Pt−Ru−B**.

Intracellular Localization Analysis by Microscopy. Specific intracellular localization of a targeted cancer drug molecule to a cellular organelle is crucial for understanding its possible mechanism of action, efficacy, and therapeutic impact. Confocal imaging is a convenient tool for cellular localization studies. The fluorescence property of the prodrug **Pt−Ru−B** (**2**) was used as a diagnostic tool for imaging A549 cancer cells on 4 h of incubation in the dark, followed by visualization using a confocal laser scanning microscope (CLSM). On 488 nm laser excitation, the cells exhibited a green emission, indicating the potential of the complex to serve as a visualizing agent. By examining different images captured with the nuclear staining blue emitting Hoechst dye, the green emission of the complex, MitoTracker deep red (MTR) as a mitochondrial marker, lysosome tracker deep red (LTR), and ER tracker deep red (ERR), it became apparent that there is no significant overlap between the complex emission and nuclear staining dye. However, the Pearson's correlation coefficients between the complex-based fluorescence and mito, lyso and ER tracker dyes are found to be ∼0.71, 0.32, and 0.15, respectively (Figure S29, Supporting Information). Pearson's correlation coefficient (PCC) value indicates preferential localization of the prodrug **Pt−Ru−B** within the mitochondria with a PCC of ∼0.71 (Figure 6).

Cellular ROS Generation. PDT involves generation of reactive oxygen species (ROS) by type-I and/or type-II photoprocesses.[56] To investigate the *in vitro* photoinduced production of ROS by **Pt−Ru−B** in A549 cells, a 2′,7′-dichlorofluorescein diacetate (DCFDA) assay was carried out. Upon cellular uptake, this cell-permeable dye undergoes hydrolysis by esterase enzymes and subsequently undergoes oxidation by ROS to form fluorescent DCF (2,7-dichloro-fluorescein).[57] The prodrug-treated A549 cells were subjected to incubation with DCFDA. Subsequently, one set of cells was exposed to visible light (400−700 nm), while the other set was left in the dark. The fluorescence intensity measurement exhibited negligible alterations within the dark-maintained set, while a noteworthy augmentation in fluorescence intensity was observed within the light-exposed set of cells, indicating ROS generation upon light exposure (Figure 7).

Wound Healing Assay. The antimetastatic potential of the prodrug **Pt−Ru−B** in A549 cells was studied using a scratch-wound healing assay to evaluate the migratory characteristics, including speed, persistence, and polarity, of a confluent monolayer of A549 cells. Specifically, the performance of A549 cells treated with the prodrug for a duration of 12

https://doi.org/10.1021/acs.inorgchem.4c03083
Inorg. Chem. 2024, 63, 17249−17262

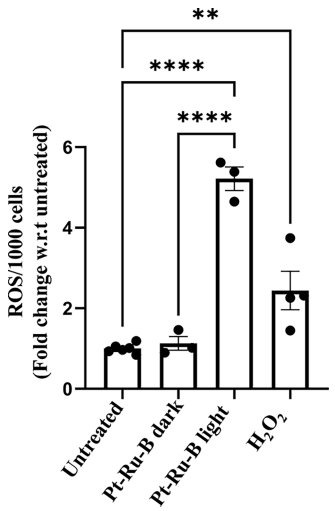

Figure 7. DCFDA assay to assess the formation of ROS in the A549 cells upon 10 min photoexposure of **Pt−Ru−B** (0.5 μM) after incubation for a duration of 4 h in dark or when maintained in dark. The bars from left are (1) cells alone, (2) cells treated with DCFDA and **Pt−Ru−B** in the dark, (3) cells treated with DCFDA and **Pt−Ru−B** in light (400−700 nm), and (4) cells treated with H_2O_2. The DCFDA fluorescent counts were subsequently normalized by cell number, and w.r.t refers to with respect to. Statistical analysis was performed using One Way ANOVA analysis and followed by Tukey's multiple comparison test (**$p < 0.01$ and ****$p < 0.00001$). All the data sets were obtained from three sets of independent experiments.

h was compared with that of the untreated cells. As shown in Figure 8, the wound borders in the control medium upon the initial scratching of the monolayer were distinctly defined. However, with the progression of time, these borders gradually migrated toward the center, resulting in a reduction of the wound area until it eventually disappeared. This observation serves as an indication of the notable migratory capacity of A549 cells under the given conditions. In contrast, following a 12 h treatment with 50 μM prodrug, a notable suppression of A549 cell migration was observed, as evidenced by the reduced closure of the wound borders. The results obtained from the wound healing assay demonstrated that the prodrug complex **Pt−Ru−B** inhibits cancer cell migration, potentially indicating antimetastatic behavior.

Mitochondrial Dysfunction. The mitochondria, known as the cellular powerhouses with ATP (adenosine triphosphate) generation, play important role in cellular metabolism.[58] However, an excessive accumulation of ROS within mitochondria could disrupt mitochondrial function, ultimately leading to a decline in ATP content. The loss of mitochondrial membrane potential ($\Delta\Psi_m$) serves as a prominent indicator of mitochondrial dysfunction. The modulation of $\Delta\Psi_m$ was evaluated using a JC-1 (5,5,6,6′-tetrachloro-1,1′,3,3′-tetraethylbenzimidazoyl-carbocyanine iodide) dye assay. Upon entry into the mitochondria, the cationic lipophilic JC-1 dye accumulates and forms red-emitting aggregates around the negatively charged mitochondria. However, in apoptotic cancer cells characterized by a collapsing $\Delta\Psi_m$, the dye fails to aggregate into red-emitting clusters and remains as a monomeric green dye dispersed within the cytoplasm. Carbonyl cyanide-4-(trifluoromethoxy)phenylhydrazone (FCCP) was used as a positive control, which induces acidification within the mitochondria, resulting in inhibition of ATP production. In the absence of photoexposure, the prodrug-treated cells exhibited an intense red emission stemming from J-aggregates. Conversely, under the influence of light exposure, cells incubated with the prodrug displayed a prominent green emission attributed to the presence of J-monomers (Figure 9a). The observations provide strong

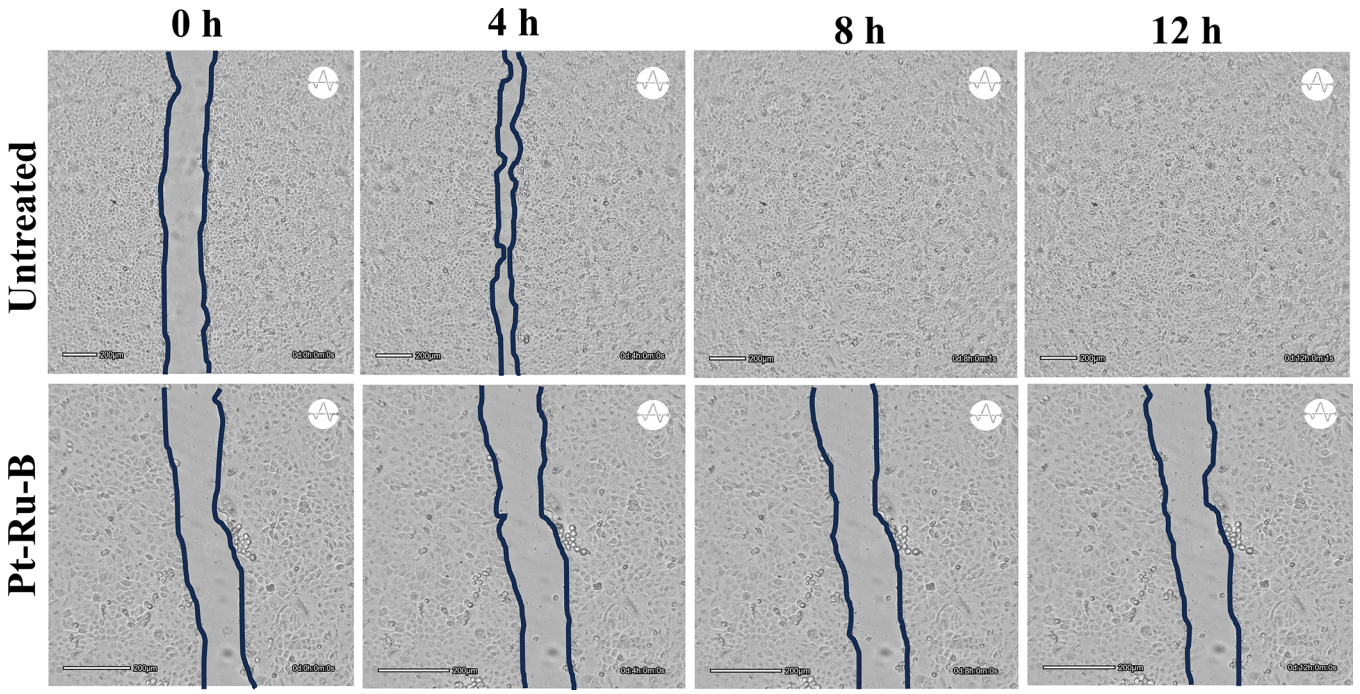

Figure 8. Presented images depict representative scratch assay results performed on A549 cancer cells to observe the impact of treating them with **Pt−Ru−B** (50 μM) on the closure of the scratch. The images captured 0, 4, 8, and 12 h after the introduction of the scratch showcase the progression of scratch closure over time. Wound borders are distinctly defined by blue borders. Scale bar: 200 μm.

https://doi.org/10.1021/acs.inorgchem.4c03083
Inorg. Chem. 2024, 63, 17249−17262

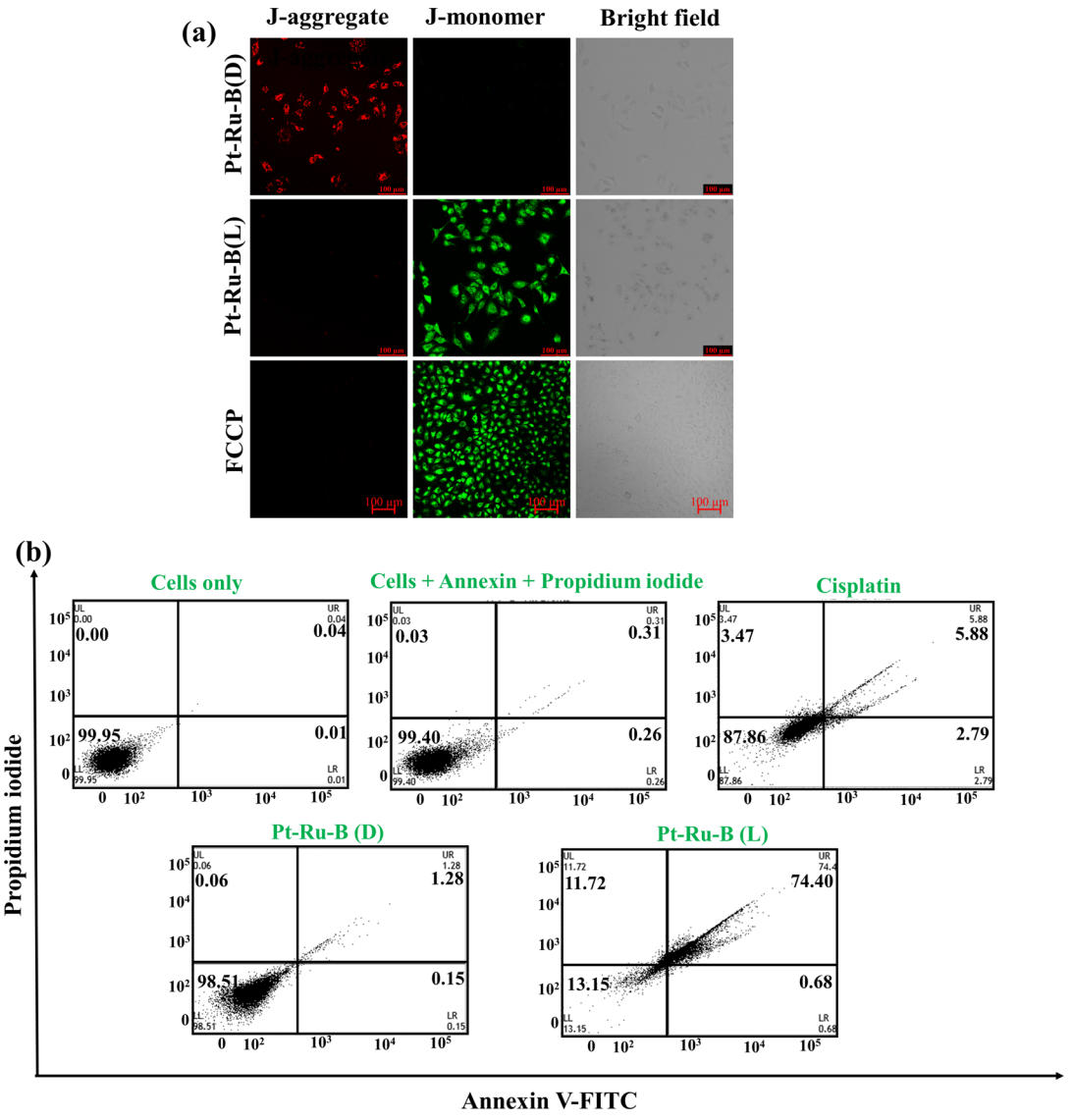

Figure 9. (a) Fluorescence images of the JC-1 dye assay at 10× magnification showing red and green fluorescence when A549 cells were incubated with **Pt−Ru−B** at 0.5 μM concentration for 4 h at 37 °C (dark) and on visible light exposure with the 400−700 nm wavelength (5 Joules/cm^2 light dose). Carbonyl cyanide-4-(trifluoromethoxy) phenylhydrazone (FCCP) was used as a positive control. Scale bar: 100 μm. (b) Dot plot of the Annexin V-FITC/propidium iodide assay using A549 cancer cells incubated with the **Pt−Ru−B**. Cisplatin was used as a positive control. The % cell population was given in the respective quadrant: lower left, live cells; lower right, early apoptotic cells; upper left, dead cells; upper right, late apoptotic cells [D, dark; L. light].

evidence that the complex selectively modulates $\Delta\Psi_m$ upon light exposure, suggesting the activation of mitochondrial driven pathways of the apoptotic process.

Cellular Apoptosis. The apoptosis induced by prodrug **Pt−Ru−B** on light irradiation was quantified from an Annexin V-FITC/propidium iodide dual staining assay. In the initial stages of apoptosis, Annexin V binds to the phosphatidylserine units on the inner cell membrane, and as the process advances, the entire complex undergoes translocation toward the outer cell membrane. In the late stages of apoptosis, the integrity of the plasma membrane becomes compromised, leading to the disintegration of cells and the formation of apoptotic vesicles or residues. During this progression, impermeable agents such as propidium iodide gain access to the inner compartments of the cell through membrane blebbing.[59] The apoptotic cells were quantified through a flow cytometry analysis. When cells exposed to light were treated with ∼0.5 μM of the prodrug, ∼75% of the cells stained for Annexin-Propidium Iodide indicate apoptosis. In contrast, within 1 h of postincubation, only ∼2% of the cells displayed apoptosis when the sample was kept in dark (Figure 9b). Positive control cisplatin (at an IC_{50} concentration) displayed ∼9% apoptosis. The results suggest the **Pt−Ru−B** induced a PDT effect through the apoptotic pathway.

Western Blotting. To gain a detailed understanding of the findings mentioned above, we conducted Western blotting to examine markers associated with cell death, particularly, cleaved caspase-7 in A549 cells. As an effector caspase facilitating cell death signaling, caspase-7 undergoes cleavage and activation, a process mediated by initiator caspase like caspase-1.[60] Caspase-7 possessing a catalytic cysteine residue within its active site enables caspase-7 to cleave various substrates, including PARP, contributing to the breakdown and destruction of the cell.[61] Figure 10 shows the presence of

https://doi.org/10.1021/acs.inorgchem.4c03083
Inorg. Chem. 2024, 63, 17249−17262

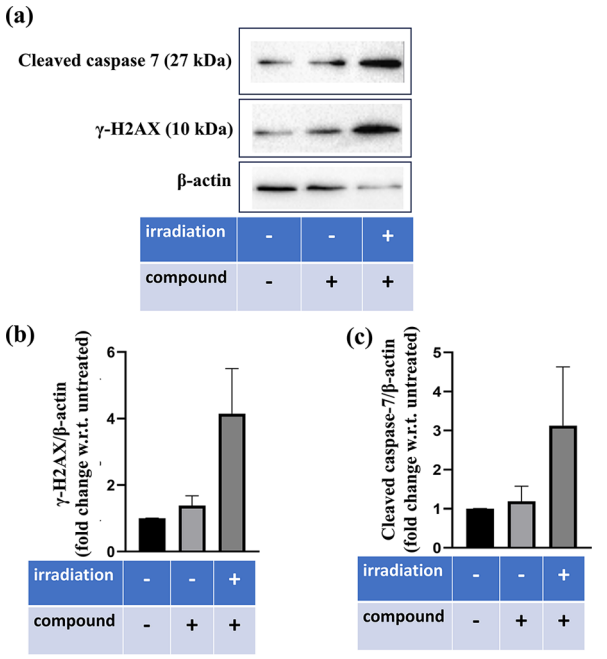

Figure 10. Western blot analysis showing overexpression of cleaved caspase-7 and γ-H2AX when A549 cells were incubated with **Pt−Ru−B** at 0.5 μM concentration for 4 h at 37 °C followed by visible light exposure with the 400−700 nm wavelength photoreactor and 5 Joules/cm^2 light dose compared to the untreated controls and dark: (a) representative Western blots, (b, c) quantitative analysis of proteins under different conditions [kDa: kilo Dalton; w.r.t. is with respect to].

cleaved caspase-7, which is significantly higher in A549 cells treated with the drug and exposed to light, in contrast to both the control group and cells that were maintained in dark. This suggests activation of apoptosis possibly through the classical DNA damage pathway. Ataxia-telangiectasia mutated proteins (ATM) play a crucial role in signaling responses to DNA damage.[62] Within chromatin, a notable target of ATM is the histone protein H2AX, and its phosphorylated form is referred to as γ-H2AX.[63] The elevation in the level of γ-H2AX serves as an indicator of DNA damage and is detectable through Western blotting. As illustrated in Figure 10a−c, the levels of γ-H2AX in cells treated with the drug under irradiation demonstrated a substantial increase compared to control cells. This suggests DNA damage was induced by the prodrug on light irradiation.

Biological Evaluation in 3D MCTs. Conventional drug screening methods using monolayer cells often face challenges in replicating the complexities and pathophysiology of tumors. Multicellular tumor spheroids (MCTs) represent cell aggregates that provide a model intermediate between monolayer cells and solid tumors. MCTs offer insights into numerous aspects of solid tumors, including characteristics such as oxygen and nutrient gradients, cell−cell matrix interactions, gene expression, and the presence of necrotic cores. To investigate the ability of drug complexes to penetrate multiple layers of cells, A549 MCTs with an approximate diameter of 200 μm were subjected to an 8 h incubation with a 30 μM concentration of complex **Pt−Ru−B**. Z-stack confocal microscopy was employed to capture images, revealing the emission of green fluorescence from multiple sections within the MCTs (Figure S30, Supporting Information). These findings affirm the complex's capability to effectively traverse the extracellular matrix barrier (ECM) and accumulate within the MCTs.

EXPERIMENTAL SECTION

The chemicals and solvents used in this study were obtained from commercial sources and used as such. **Oxoplatin** as a precursor was prepared following a literature procedure.[36] The preparations of **NHS-Bio** and **Pt-Bio** were carried out following reported protocols.[35] Details regarding the instrumentation used are given in the Supporting Information.

Materials and Methods. *Synthesis of cis-Ru(DMSO)$_4$Cl$_2$.* The synthesis was performed using a modified version of a literature procedure.[64] In a two-necked round-bottom flask equipped with a reflux condenser, 8 mL of dry DMSO was taken, and the solvent was degassed using freeze−pump−thaw cycles. Subsequently, 500 mg (∼1.89 mmol) of $RuCl_3{\cdot}xH_2O$ (39% Ru content) was added, and the reaction mixture was heated to 190 °C while being stirred for 5 min. The reaction vessel was cooled gradually to reach an ambient temperature. Following this, a volume of 30 mL of anhydrous acetone was added to the reaction mixture that was vigorously stirred for a duration of 5 min at room temperature. The resulting faint-yellow colored solid was separated by filtration, washed with diethyl ether, and subjected to vacuum drying process to isolate the product in ∼68% yield (630 mg).

*Synthesis of [Ru**L**^{1}(DMSO)Cl$_2$].* A reflux condenser was connected to a 50 mL round-bottom flask containing 20 mL of anhydrous ethanol. Then, the solvent was degassed through a series of freeze−pump−thaw cycles to remove any trapped gases. The reaction vessel was charged with 121 mg of *cis*-[Ru(DMSO)$_4$Cl$_2$] (0.25 mmol, 1.25 equiv) and 110 mg of ligand **L^1**, tpy−BOD (0.20 mmol, 1 equiv). The reaction mixture was refluxed for a period of 12 h, followed by being allowed to cool to room temperature. The solvent was removed using a rotary evaporator to obtain a residue that was subsequently subjected to purification by column chromatography using a neutral alumina column and chloroform−methanol mixture (9:1 v/v), yielding 110 mg (∼68%) of desired dark brown product.

$C_{36}H_{34}BCl_2F_2N_5ORuS$ (Mw: 805.5388). ^{1}H NMR (500 MHz, DMSO-d$_6$) δ (ppm): 9.38 (d, 2H, *J* = 5 Hz), 9.15 (s, 2H), 8.90 (d, 2H, *J* = 5 Hz), 8.52 (d, 2H, *J* = 10 Hz), 8.04 (td, 2H, *J* = 5 Hz), 7.73 (d, 2H, *J* = 10 Hz), 7.58−7.54 (m, 2H), 6.25 (s, 2H), 3.62 (s, 6H), 2.55 (s, 6H), 1.50 (s, 6H) (s, singlet; d, doublet; td, triplet of doublet; m, multiplet). ^{13}C NMR (125 MHz, DMSO-d$_6$) δ (ppm): 159.08, 158.04, 156.17, 146.75, 143.26, 137.23, 129.35, 128.89, 126.90, 124.08, 122.05, 119.22, 45.12, 14.73. ^{11}B NMR (160 MHz, DMSO-d$_6$) δ (ppm): 0.64. ^{19}F NMR (472 MHz, DMSO-d$_6$) δ (ppm): −143.57.

*Synthesis of Complex Ru−B (**1**).* A solution was prepared by dissolving 52 mg of ligand tpy−COOH (**L^2**, 0.15 mmol, 1 equiv) and 120 mg of [Ru(**L^1**)(DMSO)Cl$_2$] (0.15 mmol, 1 equiv) in 30 mL of dry and degassed ethanol in a 50 mL round-bottom flask under a nitrogen atmosphere. The resulting mixture was stirred in the dark at a temperature of 80 °C for a duration of 24 h. On completion of the reaction, the solvent was removed in a rotary evaporator. The resulting residue was dissolved in methanol, and the solution was filtered using a Celite bed to separate any undissolved impurities. The resulting filtrate was concentrated and subsequently subjected to column chromatographic purification using neutral alumina and a mixture of acetonitrile and methanol (4:1 v/v). The dark brown solid thus obtained was washed with diethyl ether, followed by vacuum drying in a desiccator containing $CaCl_2$ [Yield: ∼93 mg (63%)].

$C_{56}H_{43}BCl_2F_2N_8O_2Ru$ (Mw: 1096.8338). ^{1}H NMR (500 MHz, DMSO-d$_6$) δ (ppm): 9.63 (s, 2H), 9.51 (s, 2H), 9.17 (s, 4H), 8.72 (d, 2H, *J* = 10 Hz), 8.36 (d, 2H, *J* = 10 Hz), 8.16 (d, 2H, *J* = 10 Hz), 8.07 (s, 4H), 7.84 (d, 2H, *J* = 5 Hz), 7.59 (t, 4H, *J* = 5 Hz), 7.31−7.25 (m, 4H), 6.29 (s, 2H), 2.52 (s, 6H), 1.56 (s, 6H). ^{13}C NMR (125 MHz, DMSO-d$_6$) δ (ppm): 168.03, 158.59, 158.49, 155.77, 155.43, 152.71, 143.13, 138.54, 138.47, 136.56, 131.12, 130.31, 129.61, 128.88, 128.29, 128.11, 126.98, 125.38, 122.07, 121.51, 14.76. ^{11}B NMR (160

https://doi.org/10.1021/acs.inorgchem.4c03083
Inorg. Chem. 2024, 63, 17249−17262

MHz, DMSO-d_6) δ (ppm): 1.00. ^{19}F NMR (472 MHz, DMSO-d_6) δ (ppm): −143.64. ESI-MS (m/z) recorded in methanol: Calcd. $[M-2Cl]^{2+}$: 505.1341; Found: 505.1364. Anal. Calcd. for $C_{56}H_{43}BCl_2F_2N_8O_2Ru$ (Mw: 1096.8338) C, 62.23; H, 4.01; N, 10.37. Found: C, 62.41; H, 4.17; N, 10.45. UV−visible spectra in 10% DMSO/DPBS at pH = 7.2 [λ_{max}, nm (ε, M^{-1} cm^{-1})]: 317 (5.42×10^4), 478 (2.18×10^4), 500 (4.88×10^4) (DMSO, dimethyl sulfoxide; DPBS, Dulbecco's phosphate-buffered saline). Molar conductivity in DMF at 298 K (Λ_M/S m^2 mol^{-1}): 138.

Synthesis of Prodrug ***Pt−Ru−B*** *(**2**).* In an inert nitrogen atmosphere, **Ru−B** (115 mg, 0.11 mmol) and TBTU (2-(1*H*-benzotriazole-1-yl)-1,1,3,3-tetramethylaminium tetrafluoroborate, 51 mg, 0.16 mmol) were added to a 50 mL round-bottom flask containing 10 mL of anhydrous dimethylformamide (DMF). The resulting mixture was initially stirred at room temperature for 10 min. Triethylamine (17 mg, 0.16 mmol) was added, and the mixture was stirred for an additional 15 min. Then, the complex **Pt-Bio** (64 mg, 0.11 mmol), derived from cisplatin with a biotin ligand and axial OH ligand, was added to the reaction mixture, which was further stirred at 45 °C for a period of 48 h. The solvent was removed in a rotary evaporator, resulting in a crude mixture, which was dissolved in 10 mL of methanol and subjected to column chromatography using neutral alumina and a mixture of 4:1 (v/v) acetonitrile and methanol as the eluent. Yield: ∼68 mg (38%).

$C_{66}H_{63}BCl_4F_2N_{12}O_5RuPtS$ (Mw: 1623.1298). ^{1}H NMR (500 MHz, DMSO-d_6) δ (ppm): 9.65 (s, 2H), 9.55 (s, 2H), 9.15 (d, 4H, J = 10 Hz), 8.76 (d, 2H, J = 10 Hz), 8.71 (t, 2H, J = 10 Hz), 8.52 (d, 1H, J = 10 Hz), 8.22 (d, 1H, J = 10 Hz), 8.07 (t, 4H, J = 5 Hz), 7.86 (d, 2H, J = 10 Hz), 7.62 (d, 2H, J = 5 Hz), 7.58 (d, 2H, J = 5 Hz), 7.28 (s, 4H), 6.75−6.72 (m, 6H), 6.44−6.36 (m, 2H), 6.29 (s, 2H), 4.30 (t, 1H, J = 10 Hz), 4.15 (d, 1H, J = 5 Hz), 3.11 (d, 1H, J = 5 Hz), 2.82 (d, 2H, J = 10 Hz), 2.52 (s, 6H), 2.33−2.29 (m, 1H), 2.17 (d, 1H, J = 10 Hz), 1.61−1.34 (m, 12H). ^{13}C NMR (125 MHz, DMSO-d_6) δ (ppm): 163.19, 158.47, 155.76, 152.77, 143.13, 138.56, 131.13, 128.88, 128.26, 125.39, 125.11, 122.09, 61.51, 59.68, 55.93, 28.59, 14.76. ^{11}B NMR (160 MHz, DMSO-d_6) δ (ppm): 0.67. ^{19}F NMR (472 MHz, DMSO-d_6) δ (ppm): −143.55. ESI-MS (m/z) recorded in methanol: Calcd. $[M-2Cl]^{2+}$: 776.1457; Found: 776.1471. Anal. Calcd. for $C_{66}H_{63}BCl_4F_2N_{12}O_5RuPtS$ (Mw: 1623.1298): C, 48.84; H, 3.91; N, 10.36. Found: C, 49.07; H, 3.66; N, 10.57. UV−visible spectra in 10% DMSO/DPBS at pH = 7.2 [λ_{max}, nm (ε, M^{-1} cm^{-1})]: 316 (4.15×10^4), 477 (2.02×10^4), 500 (4.43×10^4) (DMSO, dimethyl sulfoxide; DPBS, Dulbecco's phosphate-buffered saline). Molar conductivity in DMF at 298 K (Λ_M/S m^2 mol^{-1}): 141.

Biological Experiments. Comprehensive information regarding the DNA photocleavage experiment, MTT assay, confocal imaging, JC-1 assay, Annexin V-FITC/propidium iodide assay, antimetastatic assay, Western blot, and 3D MCTs studies is given in the Supporting Information.

CONCLUSIONS

Using the concept of "Magic Bullet" in targeted therapy, a heterobimetallic Pt(IV)−Ru(II) system is designed and developed as a prodrug by incorporating biotin (vitamin B7) as an axial ligand linked to a pseudo-octahedral $5d^6$-Pt(IV) core, while a $4d^6$-Ru(II) bis-terpyridine dyad bearing a PDT-active BODIPY photosensitizer is bound to Pt(IV) as the other axial ligand. This single molecular platform exhibited good cellular uptake due to the presence of biotin moiety, while the other axially bound ruthenium(II) complex served as a photosensitizer generating singlet oxygen as ROS in high yield. Moreover, the Pt(IV) prodrug, namely, {Biotin−Pt^{IV}−(O_2C−tpy−Ru^{II}−tpy−BODIPY)} (**2**) prepared from *cis*-$[Pt(NH_3)_2Cl_2]$-derived **Oxoplatin** precursor is highly susceptible to ligand release on one-step irreversible two-electron Pt(IV)→Pt(II) reduction generating all three constituents of the prodrug. The complex on photoexposure generated singlet oxygen as the primary ROS through a type-II energy transfer process and superoxide anion radicals via a type-I electron transfer process in a minor way, as evidenced from the mechanistic DNA photocleavage studies. The prodrug also exhibited DNA photocleavage under hypoxic conditions. The metallodrug **Pt−Ru−B** demonstrated significantly enhanced chemo-PDT activity compared to the chemo-active cisplatin, the PDT-active hematoporphyrin drug Photofrin, and a 10-fold increase compared to the dyad complex **Ru−B**. This prodrug showed solution stability in the dark but was activated in the presence of cellular reducing agents, resulting in IC_{50} values in the nanomolar concentration in cancer cells while being less active in normal cells. Complex **2** showing significant mitochondrial localization and light-activated apoptotic cell death with a remarkable photocytotoxicity index value of >4500, antimetastatic properties and accumulation in 3D-multicellular tumor spheroids, exemplifies a rare and highly effective PDT agent signifying the importance of the prodrug-based approach in next generation PDT drug development.

ASSOCIATED CONTENT

Supporting Information

The Supporting Information is available free of charge at https://pubs.acs.org/doi/10.1021/acs.inorgchem.4c03083.

Detailed experimental procedures, reaction schemes, ESI-MS, NMR and electronic spectral data, cyclic voltammetry, DPBF titration plots, MTT assay plots, confocal imaging plots, theoretical calculation results, and coordinates from theoretical calculations (Schemes S1−S3; Tables S1−S4; Figures S1−S30) (PDF)

AUTHOR INFORMATION

Corresponding Authors

Deepak Kumar Saini − *Department of Developmental Biology and Genetics, Indian Institute of Science, Bangalore 560012, India; Department of Bioengineering, Indian Institute of Science, Bangalore 560012, India;* orcid.org/0000-0001-6671-7256; Phone: +91-80-22932574; Email: deepaksaini@iisc.ac.in

Akhil R. Chakravarty − *Department of Inorganic and Physical Chemistry, Indian Institute of Science, Bangalore 560012, India;* orcid.org/0000-0002-6471-9167; Phone: +91-80-22932533; Email: arc@iisc.ac.in

Authors

Arpan Bera − *Department of Inorganic and Physical Chemistry, Indian Institute of Science, Bangalore 560012, India*

Amrita Nepalia − *Department of Developmental Biology and Genetics, Indian Institute of Science, Bangalore 560012, India*

Aarti Upadhyay − *Department of Inorganic and Physical Chemistry, Indian Institute of Science, Bangalore 560012, India*

Complete contact information is available at: https://pubs.acs.org/10.1021/acs.inorgchem.4c03083

Author Contributions

A.B.—investigation (synthesis and chemical/biological aspects) and writing, A.N.—investigation (cellular), A.U.—investigation (biological), D.K.S.—review and editing (conceptual design and implementation of the cellular studies), A.R.C.—overall project administration (conceptual design and

https://doi.org/10.1021/acs.inorgchem.4c03083
Inorg. Chem. 2024, 63, 17249−17262

implementation of the bioinorganic aspects of this study), review, and editing.

Notes

The authors declare no competing financial interest.

■ ACKNOWLEDGMENTS

A.R.C. thanks the Department of Science and Technology (DST), Government of India, New Delhi, for financial support (CRG/2018/000081) and for a J. C. Bose national fellowship (SR/S2/JCB-26/2007). The authors also thank the Alexander von Humboldt (AvH) Foundation, Germany, for donation of an electrochemical system. D.K.S.'s research group is funded by DBT and SERB (CRG/2020/000239) grants. A.R.C. thanks INSA, New Delhi, for Senior Scientist fellowship (INSA/SP/SS/2021). We are thankful to Sharon for FACS data, Suchetha for confocal microscopy.

■ REFERENCES

(1) Johnstone, T. C.; Suntharalingam, K.; Lippard, S. J. The Next Generation of Platinum Drugs: Targeted Pt(II) Agents, Nanoparticle Delivery, and Pt(IV) Prodrugs. *Chem. Rev.* **2016**, *116*, 3436−3486.

(2) Kenny, R. G.; Chuah, S. W.; Crawford, A.; Marmion, C. J. Platinum(IV) Prodrugs − A Step Closer to Ehrlich's Vision? *Eur. J. Inorg. Chem.* **2017**, *2017*, 1596−1612.

(3) Ouyang, C.; Chen, L.; Rees, T. W.; Chen, Y.; Liu, J.; Ji, L.; Long, J.; Chao, H. A Mitochondria-Targeting Hetero-Binuclear Ir(III)-Pt(II) Complex Induces Necrosis in Cisplatin-Resistant Tumor Cells. *Chem. Commun.* **2018**, *54*, 6268−6271.

(4) Xu, Z.; Wang, Z.; Deng, Z.; Zhu, G. Recent Advances in the Synthesis, Stability, and Activation of Platinum(IV) Anticancer Prodrugs. *Coord. Chem. Rev.* **2021**, *442*, No. 213991.

(5) Oun, R.; Moussa, Y. E.; Wheate, N. J. The Side Effects of Platinum-Based Chemotherapy Drugs: A Review for Chemists. *Dalton Trans.* **2018**, *47*, 6645−6653.

(6) Gibson, D. Pt(IV) Anticancer Prodrugs − A Tale of Mice and Men. *ChemMedChem.* **2021**, *16*, 2188−2191.

(7) Kenny, R. G.; Marmion, C. J. Toward Multi-Targeted Platinum and Ruthenium Drugs - A New Paradigm in Cancer Drug Treatment Regimens? *Chem. Rev.* **2019**, *119*, 1058−1137.

(8) Jin, S.; Guo, Y.; Song, D.; Zhu, Z.; Zhang, Z.; Sun, Y.; Yang, T.; Guo, Z.; Wang, X. Targeting Energy Metabolism by a Platinum(IV) Prodrug as an Alternative Pathway for Cancer Suppression. *Inorg. Chem.* **2019**, *58*, 6507−6516.

(9) Chen, Q.; Yang, Y.; Lin, X.; Ma, W.; Chen, G.; Li, W.; Wang, X.; Yu, Z. Platinum(IV) Prodrugs with Long Lipid Chains for Drug Delivery and Overcoming Cisplatin Resistance. *Chem. Commun.* **2018**, *54*, 5369−5372.

(10) Bera, A.; Gautam, S.; Sahoo, S.; Pal, A. K.; Kondaiah, P.; Chakravarty, A. R. Red Light Active Pt(IV)-BODIPY Prodrug as a Mitochondria and Endoplasmic Reticulum Targeted Chemo-PDT Agent. *RSC Med. Chem.* **2022**, *13*, 1526−1539.

(11) Su, S.; Chen, Y.; Zhang, P.; Ma, R.; Zhang, W.; Liu, J.; Li, T.; Niu, H.; Cao, Y.; Hu, B.; Gao, J.; Sun, H.; Fang, D.; Wang, J.; Wang, P. G.; Xie, S.; Wang, C.; Ma, J. The Role of Platinum(IV)-Based Antitumor Drugs and the Anticancer Immune Response in Medicinal Inorganic Chemistry. A Systematic Review from 2017 to 2022. *Eur. J. Med. Chem.* **2022**, *243*, No. 114680.

(12) Krasnovskaya, O. O.; Akasov, R. A.; Spector, D. V.; Pavlov, K. G.; Bubley, A. A.; Kuzmin, V. A.; Kostyukov, A. A.; Khaydukov, E. V.; Lopatukhina, E. V.; Semkina, A. S.; Vlasova, K. Y.; Sypalov, S. A.; Erofeev, A. S.; Gorelkin, P. V.; Vaneev, A. N.; Nikitina, V. N.; Skvortsov, D. A.; Ipatova, D. A.; Mazur, D. M.; Zyk, N. V.; Sakharov, D. A.; Majouga, A. G.; Beloglazkina, E. K. Photoinduced Reduction of Novel Dual-Action Riboplatin Pt(IV) Prodrug. *ACS Appl. Mater. Interfaces* **2023**, *15*, 12882−12894.

(13) Bera, A.; Gautam, S.; Raza, K.; Kondaiah, P.; Chakravarty, A. R. Oxoplatin-B, a Cisplatin-Based Platinum (IV) Complex with Photoactive BODIPY for Mitochondria Specific " Chemo-PDT " Activity. *J. Inorg. Biochem.* **2021**, *223*, No. 111526.

(14) Deng, Z.; Wang, N.; Liu, Y.; Xu, Z.; Wang, Z.; Lau, T. C.; Zhu, G. A Photocaged, Water-Oxidizing, and Nucleolus-Targeted Pt(IV) Complex with a Distinct Anticancer Mechanism. *J. Am. Chem. Soc.* **2020**, *142*, 7803−7812.

(15) Strebhardt, K.; Ullrich, A. Paul Ehrlich's magic bullet concept: 100 years of progress. *Nat. Rev. Cancer* **2008**, *8*, 473−480.

(16) Bera, A.; Nepalia, A.; Upadhyay, A.; Saini, D. K.; Chakravarty, A. R. Biotin and Boron-Dipyrromethene-Tagged Platinum(IV) Prodrug for Cellular Imaging and Mito-Targeted Photocytotoxicity in Red Light. *Dalton Trans.* **2023**, *52*, 13339−13350.

(17) Paul, S.; Kundu, P.; Kondaiah, P.; Chakravarty, A. R. BODIPY-Ruthenium(II) Bis-Terpyridine Complexes for Cellular Imaging and Type-I/-II Photodynamic Therapy. *Inorg. Chem.* **2021**, *60*, 16178−16193.

(18) Song, H.; Cai, Z.; Li, J.; Xiao, H.; Qi, R.; Zheng, M. Light Triggered Release of a Triple Action Porphyrin-Cisplatin Conjugate Evokes Stronger Immunogenic Cell Death for Chemotherapy, Photodynamic Therapy and Cancer Immunotherapy. *J. Nanobiotechnol.* **2022**, *20*, 1−11.

(19) Wang, X.; Wang, X.; Guo, Z. Functionalization of Platinum Complexes for Biomedical Applications. *Acc. Chem. Res.* **2015**, *48*, 2622−2631.

(20) Mao, J.; Zhang, Y.; Zhu, J.; Zhang, C.; Guo, Z. Molecular Combo of Photodynamic Therapeutic Agent Silicon(IV) Phthalocyanine and Anticancer Drug Cisplatin. *Chem. Commun.* **2009**, 908−910.

(21) Imberti, C.; Zhang, P.; Huang, H.; Sadler, P. J. New Designs for Phototherapeutic Transition Metal Complexes. *Angew. Chem., Int. Ed.* **2020**, *59*, 61−73.

(22) Li, X.; Lee, S.; Yoon, J. Supramolecular Photosensitizers Rejuvenate Photodynamic Therapy. *Chem. Soc. Rev.* **2018**, *47*, 1174−1188.

(23) Wu, Y.; Li, S.; Chen, Y.; He, W.; Guo, Z. Recent Advances in Noble Metal Complex Based Photodynamic Therapy. *Chem. Sci.* **2022**, *13*, 5085−5106.

(24) Zhao, X.; Liu, J.; Fan, J.; Chao, H.; Peng, X. Recent Progress in Photosensitizers for Overcoming the Challenges of Photodynamic Therapy: From Molecular Design to Application. *Chem. Soc. Rev.* **2021**, *50*, 4185−4219.

(25) Karges, J. Clinical Development of Metal Complexes as Photosensitizers for Photodynamic Therapy of Cancer. *Angew. Chem. - Int. Ed.* **2022**, *61*, No. e202112236.

(26) Dos Santos, A. F.; De Almeida, D. R. Q.; Terra, L. F.; Baptista, M. S.; Labriola, L. Photodynamic Therapy in Cancer Treatment - an Update Review. *J. Cancer Metastasis Treat.* **2019**, *5*, 25.

(27) Yoon, I.; Li, J. Z.; Shim, Y. K. Advance in Photosensitizers and Light Delivery for Photodynamic Therapy. *Clin. Endosc.* **2013**, *46*, 7−23.

(28) Kue, C. S.; Ng, S. Y.; Voon, S. H.; Kamkaew, A.; Chung, L. Y.; Kiew, L. V.; Lee, H. B. Recent Strategies to Improve Boron Dipyrromethene (BODIPY) for Photodynamic Cancer Therapy: An Updated Review. *Photochem. Photobiol. Sci.* **2018**, *17*, 1691−1708.

(29) Bera, A.; Gautam, S.; Raza, M. K.; Pal, A. K.; Kondaiah, P.; Chakravarty, A. R. BODIPY−Dipicolylamine Complexes of Platinum-(II): X-Ray Structure, Cellular Imaging and Organelle-Specific near-IR Light Type-II PDT. *Dalton Trans.* **2022**, *51*, 3925−3936.

(30) Turksoy, A.; Yildiz, D.; Akkaya, E. U. Photosensitization and Controlled Photosensitization with BODIPY Dyes. *Coord. Chem. Rev.* **2019**, *379*, 47−64.

(31) Paul, S.; Sahoo, S.; Sahoo, S.; Jayabaskaran, C.; Chakravarty, A. R. Bichromophoric BODIPY and Biotin Tagged Terpyridyl Ruthenium(II) Complexes for Cellular Imaging and Photodynamic Therapy. *Eur. J. Inorg. Chem.* **2022**, *2022*, No. e202200487.

(32) Karges, J.; Yempala, T.; Tharaud, M.; Gibson, D.; Gasser, G. A Multi-Action and Multi-Target Ru(II)−Pt(IV) Conjugate Combining Cancer-Activated Chemotherapy and Photodynamic Therapy to

https://doi.org/10.1021/acs.inorgchem.4c03083
Inorg. Chem. 2024, 63, 17249−17262

Overcome Drug Resistant Cancers. *Angew. Chem. - Int. Ed.* **2020**, *59*, 7069−7075.
(33) Gupta, A.; Pandey, A. K.; Mondal, T.; Bhattacharya, J.; Sasmal, P. K. Multifunctional Iridium(III)-Platinum(IV) Conjugates as Potent Anticancer Theranostic Agents. *J. Med. Chem.* **2023**, *66*, 8687−8704.
(34) (a) Ma, L.; Ma, R.; Wang, Z.; Yiu, S. M.; Zhu, G. Heterodinuclear Pt(IV)-Ru(II) Anticancer Prodrugs to Combat Both Drug Resistance and Tumor Metastasis. *Chem. Commun.* **2016**, *52*, 10735−10738. (b) Babu, T.; Ghareeb, H.; Basu, U.; Schueffl, H.; Theiner, S.; Heffeter, P.; Koellensperger, G.; Metanis, N.; Gandin, V.; Ott, I.; Schmidt, C.; Gibson, D. Oral Anticancer Heterobimetallic Pt^{IV}−Au^{I} Complexes Show High In Vivo Activity and Low Toxicity. *Angew. Chemie - Int. Ed.* **2023**, *62*, No. e202217233.
(35) Muhammad, N.; Sadia, N.; Zhu, C.; Luo, C.; Guo, Z.; Wang, X. Biotin-Tagged Platinum(IV) Complexes as Targeted Cytostatic Agents against Breast Cancer Cells. *Chem. Commun.* **2017**, *53*, 9971−9974.
(36) Pathak, R. K.; Marrache, S.; Choi, J. H.; Berding, T. B.; Dhar, S. The Prodrug Platin- A: Simultaneous Release of Cisplatin and Aspirin. *Angew. Chem. - Int. Ed.* **2014**, *126*, 1994−1998.
(37) Martínez, M.; Carranza, M. P.; Massaguer, A.; Santos, L.; Organero, J. A.; Aliende, C.; De Llorens, R.; Ng-Choi, I.; Feliu, L.; Planas, M.; Rodríguez, A. M.; Manzano, B. R.; Espino, G.; Jalón, F. A. Synthesis and Biological Evaluation of Ru(II) and Pt(II) Complexes Bearing Carboxyl Groups as Potential Anticancer Targeted Drugs. *Inorg. Chem.* **2017**, *56*, 13679−13696.
(38) Jana, A.; Kundu, P.; Paul, S.; Kondaiah, P.; Chakravarty, A. R. Cobalt(III) Complexes for Light-Activated Delivery of Acetylacetonate-BODIPY, Cellular Imaging, and Photodynamic Therapy. *Inorg. Chem.* **2022**, *61*, 6837−6851.
(39) Geary, W. J. The Use of Conductivity Measurements in Organic Solvents for the Characterisation of Coordination Compounds. *Coord. Chem. Rev.* **1971**, *7*, 81−122.
(40) Peterson, J. A.; Wijesooriya, C.; Gehrmann, E. J.; Mahoney, K. M.; Goswami, P. P.; Albright, T. R.; Syed, A.; Dutton, A. S.; Smith, E. A.; Winter, A. H. Family of BODIPY Photocages Cleaved by Single Photons of Visible/Near-Infrared Light. *J. Am. Chem. Soc.* **2018**, *140*, 7343−7346.
(41) Liu, B.; Gao, Y.; Jabed, M. A.; Kilina, S.; Liu, G.; Sun, W. Lysosome Targeting Bis-Terpyridine Ruthenium(II) Complexes: Photophysical Properties and in Vitro Photodynamic Therapy. *ACS Appl. Bio Mater.* **2020**, *3*, 6025−6038.
(42) Zheng, Y. R.; Suntharalingam, K.; Johnstone, T. C.; Lippard, S. J. Encapsulation of Pt(IV) Prodrugs within a Pt(II) Cage for Drug Delivery. *Chem. Sci.* **2015**, *6*, 1189−1193.
(43) Rupp, M.; Auvray, T.; Rousset, E.; Mercier, G. M.; Marvaud, V.; Kurth, D. G.; Hanan, G. S. Photocatalytic Hydrogen Evolution Driven by a Heteroleptic Ruthenium(II) Bis(Terpyridine) Complex. *Inorg. Chem.* **2019**, *58*, 9127−9134.
(44) Mirceski, V.; Laborda, E.; Guziejewski, D.; Compton, R. G. New Approach to Electrode Kinetic Measurements in Square-Wave Voltammetry: Amplitude-Based Quasireversible Maximum. *Anal. Chem.* **2013**, *85*, 5586−5594.
(45) Frisch, M. J.; Trucks, G. W.; Schlegel, H. B.; Scuseria, G. E.; Robb, M. A.; Cheeseman, J. R.; Scalmani, G.; Barone, V.; Petersson, G. A.; Nakatsuji, H.; Li, X.; Caricato, M.; Marenich, A.; Bloino, J.; Janesko, B. G.; Gomperts, R.; Mennucci, B.; Hratchian, H. P.; Ortiz, J. V.; Izmaylov, A. F.; Sonnenberg, J. L.; Williams-Young, D.; Ding, F.; Lipparini, F.; Egidi, F.; Goings, J.; Peng, B.; Petrone, A.; Henderson, T.; Ranasinghe, D.; Zakrzewski, V. G.; Gao, J.; Rega, N.; Zheng, G.; Liang, W.; Hada, M.; Ehara, M.; Toyota, K.; Fukuda, R.; Hasegawa, J.; Ishida, M.; Nakajima, T.; Honda, Y.; Kitao, O.; Nakai, H.; Vreven, T.; Throssell, K.; Montgomery, J. A., Jr.; Peralta, J. E.; Ogliaro, F.; Bearpark, M.; Heyd, J. J.; Brothers, E.; Kudin, K. N.; Staroverov, V. N.; Keith, T.; Kobayashi, R.; Normand, J.; Raghavachari, K.; Rendell, A.; Burant, J. C.; Iyengar, S. S.; Tomasi, J.; Cossi, M.; Millam, J. M.; Klene, M.; Adamo, C.; Cammi, R.; Ochterski, J. W.; Martin, R. L.; Morokuma, K.; Farkas, O.; Foresman, J. B.; Fox, D. J. *Gaussian 09*,Rev. A.02; Gaussian, Inc.: 2016.
(46) (a) Becke, A. D. Density-Functional Thermochemistry. III. The Role of Exact Exchange. *J. Chem. Phys.* **1993**, *98*, 5648−5652. (b) Lee, C.; Yang, W.; Parr, R. G. Development of the Colle-Salvetti Correlation-Energy Formula into a Functional of the Electron Density. *Phys. Rev. B: Condens. Matter Mater. Phys.* **1988**, *37*, 785−789.
(47) Karmakar, S.; Kostrhunova, H.; Ctvrtlikova, T.; Novohradsky, V.; Gibson, D.; Brabec, V. Platinum(IV)-Estramustine Multiaction Prodrugs Are Effective Antiproliferative Agents against Prostate Cancer Cells. *J. Med. Chem.* **2020**, *63*, 13861−13877.
(48) Entradas, T.; Waldron, S.; Volk, M. The Detection Sensitivity of Commonly Used Singlet Oxygen Probes in Aqueous Environments. *J. Photochem. Photobiol. B Biol.* **2020**, *204*, No. 111787.
(49) Xie, J.; Wang, Y.; Choi, W.; Jangili, P.; Ge, Y.; Xu, Y.; Kang, J.; Liu, L.; Zhang, B.; Xie, Z.; He, J.; Xie, N.; Nie, G.; Zhang, H.; Kim, J. S. Overcoming Barriers in Photodynamic Therapy Harnessing Nano-Formulation Strategies. *Chem. Soc. Rev.* **2021**, *50*, 9152−9201.
(50) Wan, Y.; Fu, L. H.; Li, C.; Lin, J.; Huang, P. Conquering the Hypoxia Limitation for Photodynamic Therapy. *Adv. Mater.* **2021**, *33*, 1−36.
(51) Monro, S.; Colón, K. L.; Yin, H.; Roque, J.; Konda, P.; Gujar, S.; Thummel, R. P.; Lilge, L.; Cameron, C. G.; McFarland, S. A. Transition Metal Complexes and Photodynamic Therapy from a Tumor-Centered Approach: Challenges, Opportunities, and Highlights from the Development of TLD1433. *Chem. Rev.* **2019**, *119*, 797−828.
(52) Zhang, S. Q.; Meng, T. T.; Li, J.; Hong, F.; Liu, J.; Wang, Y.; Gao, L. H.; Zhao, H.; Wang, K. Z. Near-IR/Visible-Emitting Thiophenyl-Based Ru(II) Complexes: Efficient Photodynamic Therapy, Cellular Uptake, and DNA Binding. *Inorg. Chem.* **2019**, *58*, 14244−14259.
(53) Shi, G.; Monro, S.; Hennigar, R.; Colpitts, J.; Fong, J.; Kasimova, K.; Yin, H.; DeCoste, R.; Spencer, C.; Chamberlain, L.; Mandel, A.; Lilge, L.; McFarland, S. A. Ru(II) Dyads Derived from α-Oligothiophenes: A New Class of Potent and Versatile Photosensitizers for PDT. *Coord. Chem. Rev.* **2015**, *282*−*283*, 127−138.
(54) Li, H.; Bruce, G.; Childerhouse, N.; Keegan, G.; Mantovani, G.; Stolnik, S. Biotin Receptor-Mediated Intracellular Delivery of Synthetic Polypeptide-Protein Complexes. *J. Controlled Release* **2023**, *357*, 333−341.
(55) (a) Chen, J.; Lu, L.; Feng, Y.; Wang, H.; Dai, L.; Li, Y.; Zhang, P. PKD2Mediates Multi-Drug Resistance in Breast Cancer Cells through Modulation of P-Glycoprotein Expression. *Cancer Lett.* **2011**, *300*, 48−56. (b) Guo, R.; Huang, F.; Zhang, B.; Yan, Y.; Che, J.; Jin, Y.; Zhuang, Y.; Dong, R.; Li, Y.; Tan, B.; Song, R.; Hu, Y.; Dong, X.; Li, X.; Lin, N. GSH Activated Biotin-Tagged Near-Infrared Probe for Efficient Cancer Imaging. *Theranostics* **2019**, *9*, 3515−3525.
(56) Dąbrowski, J. M.; Pucelik, B.; Regiel-Futyra, A.; Brindell, M.; Mazuryk, O.; Kyzioł, A.; Stochel, G.; Macyk, W.; Arnaut, L. G. Engineering of Relevant Photodynamic Processes through Structural Modifications of Metallotetrapyrrolic Photo-sensitizers. *Coord. Chem. Rev.* **2016**, *325*, 67−101.
(57) Zhou, J.; Zhang, Y.; Yu, G.; Crawley, M. R.; Fulong, C. R. P.; Friedman, A. E.; Sengupta, S.; Sun, J.; Li, Q.; Huang, F.; Cook, T. R. Highly Emissive Self-Assembled BODIPY-Platinum Supramolecular Triangles. *J. Am. Chem. Soc.* **2018**, *140*, 7730−7736.
(58) Milane, L.; Trivedi, M.; Singh, A.; Talekar, M.; Amiji, M. Mitochondrial Biology, Targets, and Drug Delivery. *J. Controlled Release* **2015**, *207*, 40−58.
(59) Upadhyay, A.; Kundu, P.; Ramu, V.; Kondaiah, P.; Chakravarty, A. R. BODIPY-Tagged Platinum(II) Curcumin Complexes for Endoplasmic Reticulum-Targeted Red Light PDT. *Inorg. Chem.* **2022**, *61*, 1335−1348.
(60) McIlwain, D. R.; Berger, T.; Mak, T. W. Caspase Functions in Cell Death and Disease. *Cold Spring Harb. Perspect. Biol.* **2013**, *5*, No. a008656.

https://doi.org/10.1021/acs.inorgchem.4c03083
Inorg. Chem. 2024, 63, 17249−17262

(61) Li, W.; Jiang, G. B.; Yao, J. H.; Wang, X. Z.; Wang, J.; Han, B. J.; Xie, Y. Y.; Lin, G. J.; Huang, H. L.; Liu, Y. J. Ruthenium(II) Complexes: DNA-Binding, Cytotoxicity, Apoptosis, Cellular Localization, Cell Cycle Arrest, Reactive Oxygen Species, Mitochondrial Membrane Potential and Western Blot Analysis. *J. Photochem. Photobiol., B* **2014**, *140*, 94−104.
(62) Shiloh, Y. Ataxia-Telangiectasia and the Nijmegen Breakage Syndrome: Related Disorders but Genes Apart. *Annu. Rev. Genet.* **1997**, *31*, 635−662.
(63) Goldstein, M.; Kastan, M. B. The DNA Damage Response: Implications for Tumor Responses to Radiation and Chemotherapy. *Annu. Rev. Med.* **2015**, *66*, 129−143.
(64) Evans, I. P.; Spencer, A.; Wilkinson, G. Dichlorotetrakis-(dimethy1 sulfoxide)ruthenium(II) and its Use as a Source Material for Some New Ruthenium(II) Complexes. *J. Chem. Soc., Dalton Trans.* **1973**, *204*, 204−209.

https://doi.org/10.1021/acs.inorgchem.4c03083
Inorg. Chem. 2024, 63, 17249−17262